Volume 2 | Number 12 | December 2015

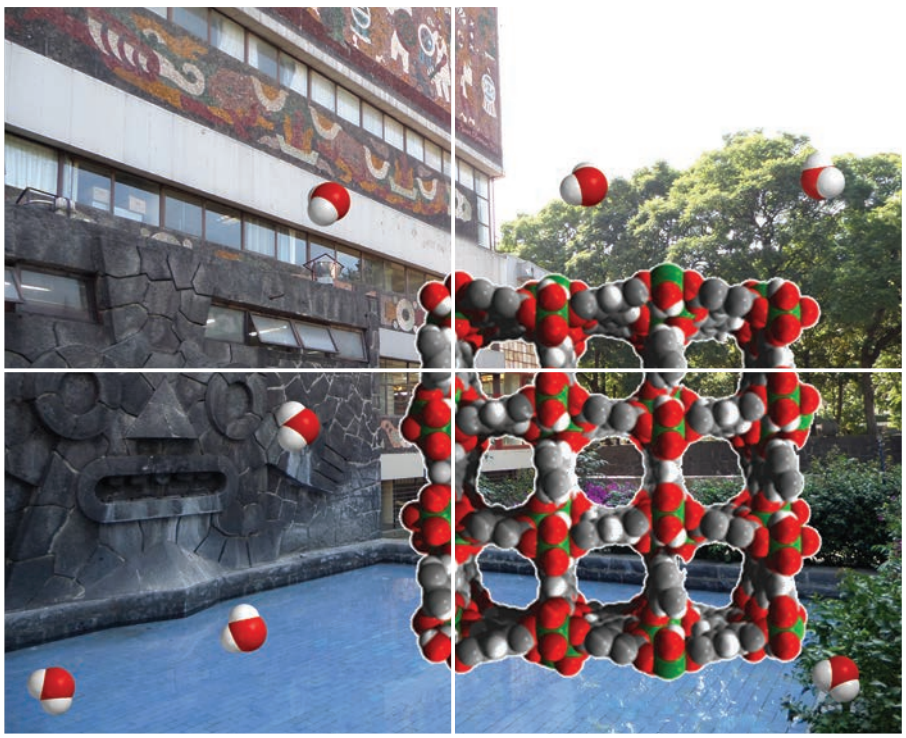

INORGANIC CHEMISTRY

FRONTIERS

Chinese Chemical Society
PEKING UNIVERSITY 1898
ROYAL SOCIETY OF CHEMISTRY

http://rsc.li/frontiers-inorganic

INORGANIC CHEMISTRY
FRONTIERS

RESEARCH ARTICLE

Cite this: *Inorg. Chem. Front.*, 2015, **2**, 1101

Cation reduction and comproportionation as novel strategies to produce high voltage, halide free, carborane based electrolytes for rechargeable Mg batteries†

Scott. G. McArthur,‡[a] Linxiao Geng,‡[b] Juchen Guo*[b,c] and Vincent Lavallo*[a]

Received 3rd September 2015,
Accepted 14th October 2015

DOI: 10.1039/c5qi00171d

rsc.li/frontiers-inorganic

Here we describe the cation reduction and comproportionation as novel routes to synthesize electrolytes for rechargeable Mg-ion batteries. Reduction of the ammonium cation in $[HNMe_3^{1+}][HCB_{11}H_{11}^{1-}]$ with metallic Mg affords the halide free carborane salt $[Mg^{2+}][HCB_{11}H_{11}^{1-}]_2$. Comproportionation of $[Mg^{2+}][HCB_{11}H_{11}^{1-}]_2$ with $MgPh_2$ affords the novel monocationic electrolyte $[MgPh^{1+}][HCB_{11}H_{11}^{1-}]$, which reversibly deposits/strips Mg with a remarkable oxidative stability of 4.6 V *vs.* $Mg^{0/+2}$.

Over the last decade there has been an explosion of technological advances in rechargeable portable devices and electric vehicles. However, innovations that reduce the cost, improve the sustainability, and increase the storage capacity offered by the state-of-the-art Li-ion technology have not kept pace with this revolution.[1] Li-ion batteries are also disadvantageous, since lithium is expensive, not earth abundant (Li^+, 0.0017% of the earth's crust), very pyrophoric, and prone to hazardous dendrite formation.[2] To avoid dendrite formation, intercalation type anodes (*e.g.* graphite) are used in current Li-ion batteries, significantly reducing the possible energy capacity both gravimetrically and volumetrically. Mg-based batteries[3] are an attractive alternative to Li-ion systems because Mg is less expensive, much more abundant (4% of the earth's crust), more tolerant of air, and does not form dendrites. The absence of dendrite formation during Mg deposition allows the utilization of pure Mg anodes, which drastically increases the energy storage capacity of the battery. In addition, since Mg is a small divalent atom it can store twice the amount of electrons compared to Li.

In contrast to Li, Mg has a unique chemistry that limits suitable solvents to aprotic and relatively non-polar ethers (*e.g.* dimethoxyethane (DME), and higher glymes).[3b,c] Mg salts that are analogous to Li salts, such as magnesium hexafluorophosphate ($[Mg][PF_6]_2$), are not suitable solutes for Mg-ion electrolytes because the anions of these salts degrade during the required electrochemical processes and form a solid organic/inorganic film covering the Mg anode. Due to its divalency, Mg ions cannot penetrate this solid layer, hence reversible Mg deposition and stripping cannot be achieved utilizing these common salts.

While Grignard reagents (RMgX) were observed to reversibly deposit/strip Mg in as early as the 1920s,[4] they are not suitable electrolytes due to their reducing power and poor electrochemical stability. The first breakthrough in electrolyte development was made by Gregory[5] in 1990 who reported that non-reducing Mg organo-borates/aluminates, such as $[Mg][BBu_2Ph_2]_2$, would reversibly deposit/strip Mg; however, these systems suffer from low oxidative stability (<2 V *vs.* $Mg^{0/+2}$). Based on this observation Aurbach and coworkers[3a,c] introduced a transmetalation strategy between Lewis basic diorganomagnesium reagents (MgR_2) and Lewis acidic aluminum species ($AlCl_2R$), to produce Mg organo-haloaluminate electrolytes (Fig. 1, top). The inorganic chloride was found to be the only suitable anionic supporting ligand for Mg ions in these systems. The solutions of these electrolytes are complex equilibrium mixtures of multiple neutral and ionic compounds. The optimal mixtures have an enhanced electrochemical stability (up to 3.3 V *vs.* $Mg^{0/+2}$ on a Pt current collector)[3c] and lead to the first example of a working rechargeable Mg battery.[3a] One drawback of this transmetalation strategy is that it prohibits the exploration of organic anionic supporting ligands, which might produce distinct or perhaps superior monocationic Mg fragments. In addition, the inherent requirement for the introduction of other metals can result in unwanted side reactions,

[a]*Department of Chemistry, University of California Riverside, Riverside, CA 92521, USA. E-mail: vincent.lavallo@ucr.edu*
[b]*Department of Chemical and Environmental Engineering, University of California Riverside, Riverside, CA 92521, USA. E-mail: jguo@engr.ucr.edu*
[c]*Materials Science and Engineering Program, University of California Riverside, Riverside, CA 92521, USA*

†Electronic supplementary information (ESI) available: Details of experimental procedures, NMR spectra of the synthesized organo-Mg compounds, and electrochemical characterization. CCDC 1403836 for **1[MgPh^{1+}]**. See DOI: 10.1039/c5qi00171d

‡Designates S.G.M. and L.G. have equal author contributions.

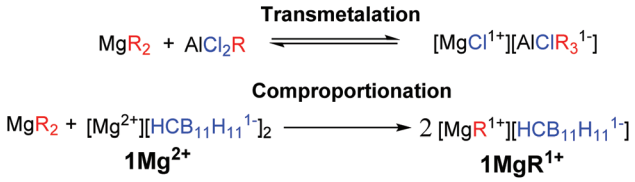

Fig. 1 A simplified chemical equation representing a transmetalation reaction to form a generic organo-haloaluminate electrolyte (top). A general equation for a comproportionation reaction between a diorganomagnesium reagent and a simple magnesium salt of a weakly coordinating anion (bottom). R = alkyl or aryl.

such as the electrochemical deposition of aluminium.[3c] Moreover, the presence of halide ions is undesirable in practical Mg batteries because they lead to corrosion of the non-noble metal battery components.[6] Therefore, over the last several years there has been a significant effort to discover suitable electrolyte systems that are both halide free and have feature enhanced electrochemical performance.[7]

Here we describe a unique and economical approach to produce halide free electrolytes for Mg batteries, namely the chemical reduction of reactive cations with the Mg metal. In addition, we introduce a novel comproportionation strategy between a diorganomagnesium reagent and a simple halide free Mg salt of a weakly coordinating carborane anion **1**[Mg^{2+}] to produce a highly electrochemically stable monocationic electrolyte **1**[MgR^{1+}], featuring an organic ligand. This strategy is adventitious to transmetalation, since only Mg reagents are used.

One of the most inert and weakly coordinating polyatomic anions is the icosahedral carborane anion $HCB_{11}H_{11}^{1-}$ (**1**) (Fig. 2).[8] Classically, derivatives of this cluster have been utilized as spectator anions for reactive molecular species[9] and more recently as ligand substituents.[10] Elegant work by Boeré and Knapp[11] has shown that the measured oxidation potential of **1** is +2.35 V *versus* $Fc^{0/+}$ (approx. +5.36 V *vs.* $Mg^{0/+2}$) in liquid SO_2. The reduction potential of **1** is estimated to be well below −4 V *versus* $Fc^{0/+}$ (below −1 V *vs.* $Mg^{0/+2}$), but has not been measured, since no suitable solvent has been found. Such carborane anions should be ideal components for Mg battery electrolytes. Very recently Mohtadi and coworkers[7a] at the Toyota Research Center reported the preparation of halide free **1**[Mg^{2+}] *via* salt metathesis of $MgBr_2$ with non-commercially available **1**[Ag^{1+}] in THF (Fig. 2, left). From an economic perspective this strategy is not practical since two equivalents of a precious metal salt by-product (AgBr) are produced per molar equivalent of Mg^{2+}. Moreover, the crude **1**[Mg^{2+}] product is not sufficiently pure for electrochemistry without an unusual purification procedure. Sometime ago, we independently prepared **1**[Mg^{2+}] by a superior and much simpler method namely the direct chemical reduction of **1**[$HNMe_3^{1+}$] with the Mg metal (Fig. 2, right). Here the metallic Mg transfers two electrons to two $HNMe_3^{1+}$ molecules with subsequent evolution of volatile H_2 and NMe_3 as the only by-products. This method results in quantitative conversion of commercially available **1**[$HNMe_3^{1+}$] to **1**[Mg^{2+}] in a single simple step and avoids the formation of precious metal by-products. Moreover, the material is sufficiently pure for electrochemical studies, *vide infra*. As observed by Mohtadi,[7a] when produced in THF, **1**[Mg^{2+}] precipitates as a completely insoluble white powder, which is only appreciably soluble in triglyme and tetraglyme. In these solvents this electrolyte shows electrochemical stability up to the limit of the solvent (3.8 V *vs.* $Mg^{0/+2}$) but only moderate conductivity. The modest conductivity of **1**[Mg^{2+}], is likely due to the strong coulombic attraction between the dipositively charged Mg^{2+} ion and the carborane anions.

Seeking to improve the solubility and conductivity of this electrolyte we envisioned designing a system with reduced coulombic interactions. Furthermore, enhanced solubility might offer the possibility of utilizing more oxidatively stable solvents, which could lead to higher voltage electrolyte systems. We hypothesized that attaching a suitable organic ligand (R^-) to the Mg^{2+} ion in **1**[Mg^{2+}] would produce unique carborane electrolytes **1**[MgR^{1+}]. We also desired a method that could potentially be used to rapidly create a library of electrochemically distinct Mg electrolytes without the introduction of potential contaminants, as in transmetalation reactions. It was reasoned that treatment of Lewis acidic **1**[Mg^{2+}] with an equal molar amount of a halide free Lewis basic diorganomagnesium reagent MgR_2 would result in comproportionation to afford **1**[MgR^{1+}] species. Inspired by Aurbach's all phenyl complex electrolyte (APC),[3c] which features an oxidation resistant phenyl substituent, we predicted that readily available $MgPh_2$ would be an ideal reactant. Indeed, treatment of a suspension of **1**[Mg^{2+}] in DME with a DME solution of $MgPh_2$ instantly solubilizes the mixture suggesting that a reaction occurred (Fig. 3). The analysis of the solution by ^1H NMR spectroscopy (ESI†) shows the disappearance of resonances associated with

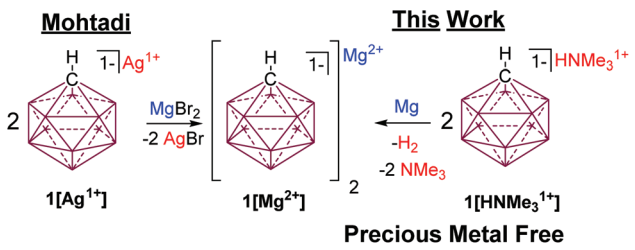

Fig. 2 Mohtadi's route to **1**[Mg^{2+}] requires the use of a precious metal (left). Halide and Ag free synthesis of **1**[Mg^{2+}] by cation reduction with Mg.

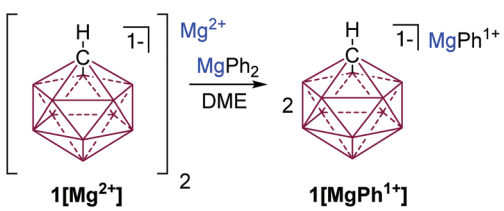

Fig. 3 Comproportionation of **1**[Mg^{2+}] and $MgPh_2$ to produce **1**[$MgPh^{+1}$] (top).

$MgPh_2$ and the formation of a single new product with aromatic resonances, consistent with the formation of **1[MgPh^{1+}]**.

In addition, the ^{13}C NMR spectrum (ESI†) shows a distinct quaternary aryl resonance at 169.8 ppm, which is 10 ppm upfield with respect to $MgPh_2$ and suggests that the aryl substituent is bound to a more electrophilic Mg center.[12] Variable temperature NMR experiments to a temperature as low as −50 °C, show the presence of only single molecular species, which demonstrates the absence of an observable Schlenk-like equilibrium on the NMR time scale. The apparent absence of an observable Schlenk equilibrium highlights the poor nucleophilicity of the carborane anion compared to the halide ions present in Grignard reagents and organo-haloaluminates. The ^{11}B NMR of **1[MgPh^{1+}]** (ESI†) is identical to **1[Mg^{2+}]**, which suggests that the carborane anion **1** has no interaction with the [**MgPh^{1+}**] cation. Although the data is not of sufficient quality to accurately discuss bond lengths and angles, a single crystal X-ray diffraction study confirms the structure of **1[MgPh^{1+}]** (Fig. 4). In the solid-state, the Mg center is octahedrally coordinated to the Ph group, two molecules of chelating DME, and a single molecule of THF. The closest approach between the carborane anion **1** and the Mg center is approximately 6.7 angstroms, which is out of the range for both covalent and van der Waals interactions.

The **1[MgPh^{1+}]** electrolyte in DME demonstrates an excellent room temperature conductivity. As shown in the ESI,† the conductivity of the **1[MgPh^{1+}]** electrolyte in DME increases as a function of salt concentration. At 0.4 M, the conductivity is 1.24×10^{-2} S cm^{-1}, which is more than 4 times higher than the maximum conductivity of **1[Mg^{2+}]** reported by Mohtadi (0.75 M in triglyme, 2.9×10^{-3} S cm^{-1}).[7a] As demonstrated by cyclic voltammetry (CV), **1[MgPh^{1+}]** also shows reversible Mg deposition/stripping and excellent anodic stability on various metal surfaces. As shown in Fig. 5a, CV scans show facile Mg deposition and stripping on all working electrodes (WE) including platinum (Pt), glassy carbon (GC), titanium (Ti), nickel (Ni), 316 stainless steel (SS) with low overpotentials (250 to 300 mV depending on the surface). Metallic Mg deposition was confirmed by scanning electron microscopy and X-ray diffraction studies (ESI†). Impressively, anodic scans of the electrolyte (inset in Fig. 5a) demonstrate the unprecedented oxidative stability of **1[MgPh^{1+}]** with various WEs using a scan rate of 5 mV s^{-1}. Enlargement of the 3.5 to 5.0 V region of the anodic scan shows the oxidative onset potentials (inset). This electrolyte is stable up to 4.6 V *vs.* $Mg^{0/+2}$ on both Pt and GC, rendering it by far the most oxidatively stable Mg-ion electrolyte reported to date. The anodic stability is 4.2 V on Ti and 3.5 V on both SS and Ni. While the oxidative stability of the carborane anion **1** is not surprising given the data reported by Boeré and Knapp, the electrochemical stability of the novel cation [**MgPh^{1+}**] containing an organic ligand is truly remarkable. The Mg deposition/stripping CV cycling curves and cycling coulombic efficiency are shown in Fig. 5b.

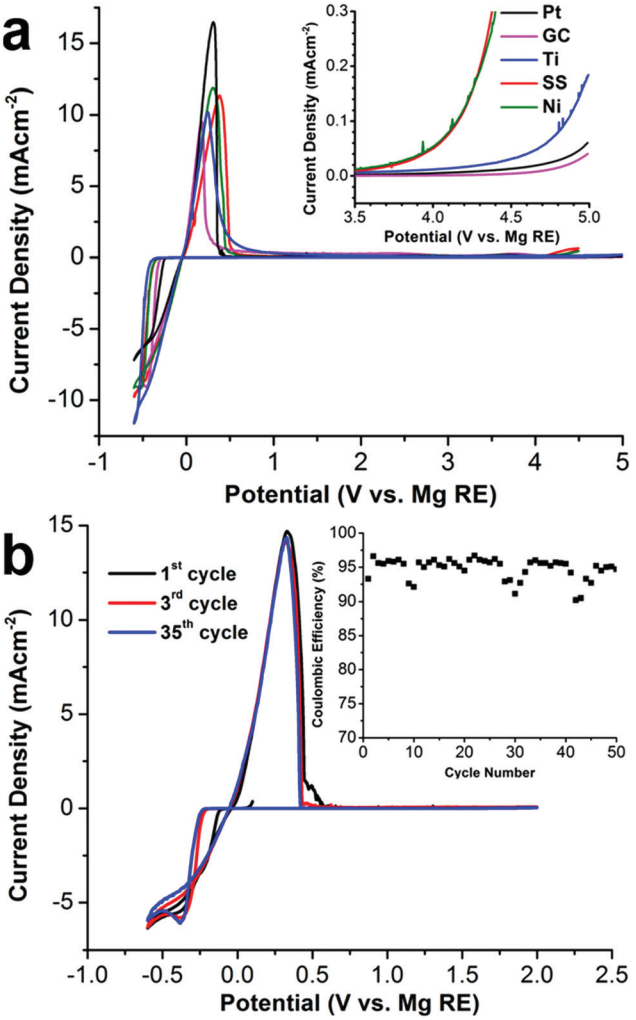

Fig. 5 (a) First CV scan of 0.4 M **1[MgPh^{1+}]** in DME on various WEs using scan rate of 5 mV s^{-1}. Enlargement of 3.5 to 5.0 V region of the anodic scan shows the oxidative onset potentials (inset). (b) Selected CV cycling curves of Mg deposition/stripping on a Pt working electrode with a 5 mV s^{-1} scan rate. The inset shows the coulombic efficiency as a function of the CV cycle number.

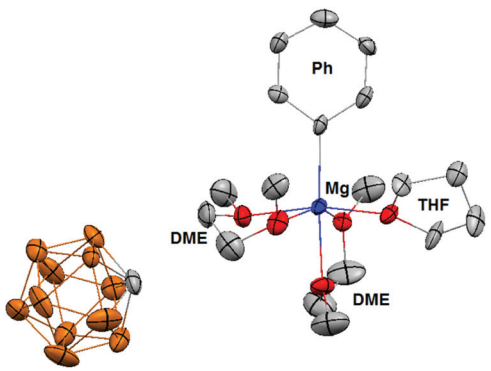

Fig. 4 Solid state-structure of **1[MgPh^{1+}]** with a THF and two coordinated DME molecules. Hydrogen atoms and two molecules of cocrystallized toluene are omitted for clarity and thermal ellipsoids are drawn at the 50% probability level (color code: blue = Mg; grey = carbon; brown = boron; red = oxygen).

The efficiency of the first cycle on Pt WE is 93.0%, which improves to 95.0% in the following 50 cycles. The average coulombic efficiency of Mg deposition/stripping on Ni, Ti, and SS is also measured with a galvanostatic cycling method (ESI†) as 95.3%, 93.7%, and 91.7%, respectively. The feasibility of **1[MgPh^{1+}]** in DME as an electrolyte in rechargeable Mg-ion batteries was demonstrated using coin cells with a Mg metal anode and the standard Mo_6S_8 cathode (ESI†). The Mg-Mo_6S_8 batteries demonstrate performance consistent with other reported studies.[13]

Conclusions

The manuscript above introduces several key advances that pave the way for the development of practical high capacity Mg batteries. The reduction of reactive cations to form halide free electrolytes should be a broadly applicable method for the preparation of any electrolytes that will be suitable for Mg batteries. Since the anionic component of competent electrolytes must be chemically inert towards Mg, this method also serves as a chemical test to ensure electrolyte compatibility with the anode. The comproportionation strategy serves as an entry way into sophisticated highly oxidatively stable monocationic carborane salts **1[MgR^{1+}]** containing organic ligands, as exemplified by the preparation of **1[MgPh^{1+}]**. Lastly, access to electrolytes that have oxidative stability beyond 4.5 V creates a novel paradigm for discovering entirely new high voltage cathode materials for the development of practical high capacity Mg-ion batteries.

Acknowledgements

This material is based on work supported in part by the National Science Foundation (DMR-1508537).

Notes and references

1 R. Van Noorden, *Nature*, 2014, **507**, 26.

2 H. Kim, G. Jeong, Y.-U. Kim, J.-H. Kim, C.-M. Park and H.-J. Sohn, *Chem. Soc. Rev.*, 2013, **42**, 9011.

3 (*a*) D. Aurbach, Z. Lu, A. Schechter, Y. Gofer, H. Gizbar, R. Turgeman, Y. Cohen, M. Moshkovich and E. Levi, *Nature*, 2000, **407**, 724; (*b*) R. Mohtadi and F. Mizuno, *Beilstein J. Nanotechnol.*, 2014, **5**, 1291; (*c*) H. D. Yoo, I. Shterenberg, Y. Gofer, G. Gershinsky, N. Pour and D. Aurbach, *Energy Environ. Sci.*, 2013, **6**, 2265; (*d*) J. Muldoon, C. B. Bucur, A. G. Oliver, T. Sugimoto, M. Matsui, H. S. Kim, G. D. Allred, J. Zajicek and Y. Kotani, *Energy Environ. Sci.*, 2012, **5**, 5941; (*e*) D. Aurbach, G. S. Suresh, E. Levi, A. Mitelman, O. Mizrahi, O. Chusid and M. Brunelli, *Adv. Mater.*, 2007, **19**, 4260.

4 (*a*) L. W. Gaddum and H. E. French, *J. Am. Chem. Soc.*, 1927, **49**, 1295; (*b*) W. V. Evans and F. H. Lee, *J. Am. Chem. Soc.*, 1934, **56**, 654.

5 T. D. Gregory, R. J. Hoffman and R. C. Winterton, *J. Electrochem. Soc.*, 1990, **137**, 775.

6 J. Muldoon, C. B. Bucur, A. G. Oliver, J. Zajicek, G. D. Allred and W. C. Boggess, *Energy Environ. Sci.*, 2013, **6**, 482.

7 (*a*) O. Tutusaus, R. Mohtadi, T. S. Arthur, F. Mizuno, E. G. Nelson and Y. V. Sevryugina, *Angew. Chem., Int. Ed.*, 2015, **54**, 7900; (*b*) S. Su, Z. Huang, Y. NuLi, F. Tuerxun, J. Yang and J. Wang, *Chem. Commun.*, 2015, **51**, 2641; (*c*) J. Zhu, Y. Guo, J. Yang, Y. Nuli, F. Zhang, J. Wang and S.-i. Hirano, *J. Power Sources*, 2014, **248**, 690; (*d*) T. J. Carter, R. Mohtadi, T. S. Arthur, F. Mizuno, R. Zhang, S. Shirai and J. W. Kampf, *Angew. Chem., Int. Ed.*, 2014, **53**, 3173; (*e*) S.-Y. Ha, Y.-W. Lee, S. W. Woo, B. Koo, J.-S. Kim, J. Cho, K. T. Lee and N.-S. Choi, *ACS Appl. Mater. Interfaces*, 2014, **6**, 4063; (*f*) R. Mohtadi, M. Matsui, T. S. Arthur and S.-J. Hwang, *Angew. Chem., Int. Ed.*, 2012, **51**, 9780.

8 (*a*) C. Douvris and J. Michl, *Chem. Rev.*, 2013, **113**, PR179; (*b*) D. Olid, R. Nunez, C. Vinas and F. Teixidor, *Chem. Soc. Rev.*, 2013, **42**, 3318; (*c*) P. Farras, E. J. Juarez-Perez, M. Lepsik, R. Luque, R. Nunez and F. Teixidor, *Chem. Soc. Rev.*, 2012, **41**, 3445; (*d*) M. Scholz and E. Hey-Hawkins, *Chem. Rev.*, 2011, **111**, 7035; (*e*) Y. Li, P. J. Carroll and L. G. Sneddon, *Inorg. Chem.*, 2008, **47**, 9193.

9 (*a*) C. A. Reed, *Acc. Chem. Res.*, 2009, **43**, 121; (*b*) C. Douvris and O. V. Ozerov, *Science*, 2008, **321**, 1188.

10 (*a*) A. R. Popescu, F. Teixidor and C. Viñas, *Coord. Chem. Rev.*, 2014, **269**, 54; (*b*) A. M. Spokoyny, *Pure Appl. Chem.*, 2013, **85**, 903; (*c*) J. Estrada, D. H. Woen, F. S. Tham, G. M. Miyake and V. Lavallo, *Inorg. Chem.*, 2015, **54**, 5142; (*d*) M. J. Asay, S. P. Fisher, S. E. Lee, F. S. Tham, D. Borchardt and V. Lavallo, *Chem. Commun.*, 2015, **51**, 5359; (*e*) J. Estrada, S. E. Lee, S. G. McArthur, A. El-Hellani, F. S. Tham and V. Lavallo, *J. Organomet. Chem.*, 2015, DOI: 10.1016/j.jorganchem.2015.05.008; (*f*) A. El-Hellani, C. E. Kefalidis, F. S. Tham, L. Maron and V. Lavallo, *Organometallics*, 2013, **32**, 6887; (*g*) A. El-Hellani and V. Lavallo, *Angew. Chem., Int. Ed.*, 2014, **53**, 4489; (*h*) V. Lavallo, J. H. Wright, F. S. Tham and S. Quinlivan, *Angew. Chem., Int. Ed.*, 2013, **52**, 3172; (*i*) M. Asay, C. E. Kefalidis, J. Estrada, D. S. Weinberger, J. Wright, C. E. Moore, A. L. Rheingold, L. Maron and V. Lavallo, *Angew. Chem., Int. Ed.*, 2013, **52**, 11560.

11 R. T. Boeré, C. Bolli, M. Finze, A. Himmelspach, C. Knapp and T. L. Roemmele, *Chem. – Eur. J.*, 2013, **19**, 1784.

12 Similar to aryl Li reagents, aryl Mg reagents display very downfield shifted resonances for the carbon bound to the metal. This can be explained by a reduction in π-delocalization as a result of electrostatic repulsion between the carbanion "like" center and the π-electrons. A cationic metal center reduces this effect. For a discussion, see: J. A. Ladd, *Spectrochim. Acta*, 1966, **22**, 1157.

13 (*a*) Y. Cheng, L. R. Parent, Y. Shao, C. Wang, V. L. Sprenkle, G. Li and J. Liu, *Chem. Mater.*, 2014, **26**, 4904; (*b*) T. Liu, Y. Shao, G. Li, M. Gu, J. Hu, S. Xu, Z. Nie, X. Chen, C. Wang and J. Liu, *J. Mater. Chem. A*, 2014, **2**, 3430; (*c*) P. Saha, P. H. Jampani, M. K. Datta, C. U. Okoli, A. Manivannan and P. N. Kumta, *J. Electrochem. Soc.*, 2014, **161**, A593.

Electronic Supplementary Material (ESI) for Inorganic Chemistry Frontiers.

Electronic Supplementary Information

Cation Reduction and Comproportionation as Novel Strategies to Produce High Voltage, Halide Free, Carborane Based Electrolytes for Rechargeable Mg Batteries

Scott G. McArthur, Linxiao Geng, Juchen Guo,* Vincent Lavallo*

Table of Contents

General Considerations

Unless otherwise stated all manipulations were carried out using standard Schlenk or glovebox techniques (O_2, H_2O < 1ppm) under a dinitrogen or argon atmosphere. Solvents were dried on K, Na or CaH_2, and distilled under argon before use. Ph_2Mg was prepared according to literature methods.[1] Reagents were purchased from commercial vendors and used without further purification. NMR spectra were recorded on Bruker Avance 300 MHz, Varian Inova 300 MHz, Varian Inova 400 MHz, or Varian Inova 500 MHz spectrometers. NMR chemical shifts are reported in parts per million (ppm). ^{1}H NMR and ^{13}C NMR chemical shifts were referenced to residual solvent. ^{11}B NMR chemical shifts were externally referenced to BF_3OEt_2.

Synthesis of 1[Mg^{2+}]

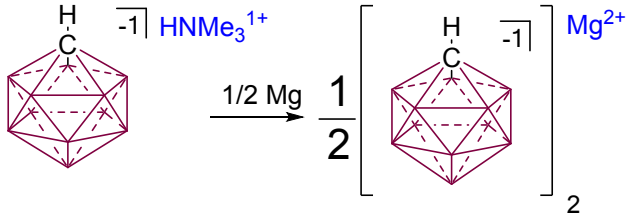

1[$HNMe_3^{1+}$] **1[Mg^{2+}]**

1[$HNMe_3^{1+}$] (2.0 g, 10.3 mmol) was added to a suspension of Mg powder (4.0 g, 165 mmol) in a minimal amount of THF (5mL) and the resulting suspension was stirred for 1 hr. After 1 hr, additional THF (30mL) was added and the suspension was left to stir for 24 hours. The THF solution was then filtered through a medium porosity fritted funnel. The collected precipitate of white powder and excess magnesium was washed with DME, dissolving the white powder of the collected precipitate. Unreacted magnesium powder was collected and reused. The DME solvent was removed under high vacuum, resulting in compound **1[Mg^{2+}]** as a white powder in 91% yield (5.44 g 9.37 mmol) (**Note:** Mg^{2+} counter cations contain 3 coordinated DME molecules). Once dried, compound **1[Mg^{2+}]** is only soluble in DME at cold temperatures -30°C (**Note:** Mg^{2+} counter cation is coordinated to three DME molecules). The reaction progress is monitored using ^{1}H NMR by the loss of trimethyl ammonium counter cation peak at δ = 3.19 ppm in acetone-d_6. ^{1}H NMR (300 MHz, acetone-d_6, 25°C): δ = 3.46 (s, 4H), 3.28 (s, 6H), 2.50-0.75 (bm, 11 H, B-*H*) ppm; ^{1}H{^{11}B} NMR (300 MHz, acetone-d_6, 25 °C): δ = 3.46 (s, 4H), 3.28 (s, 6H), 2.22 (s, 1H, B-*H*); ^{11}B {^{1}H} NMR (96 MHz, acetone-d_6, 25 °C): δ = -3.2, -9.6, -12.6 ppm.

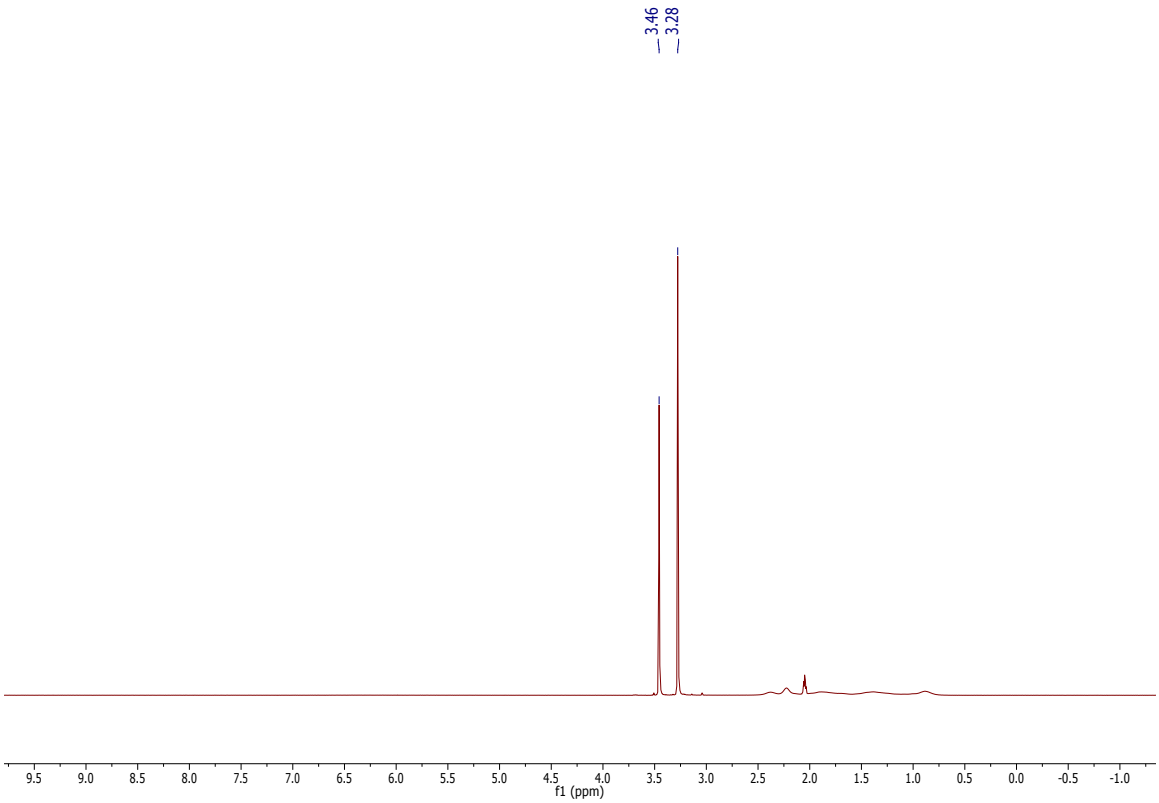

Figure S1. ^{1}H NMR of **1[Mg^{2+}]** in acetone-d_6 (**Note:** peaks at 3.45 and 3.28 ppm are DME).

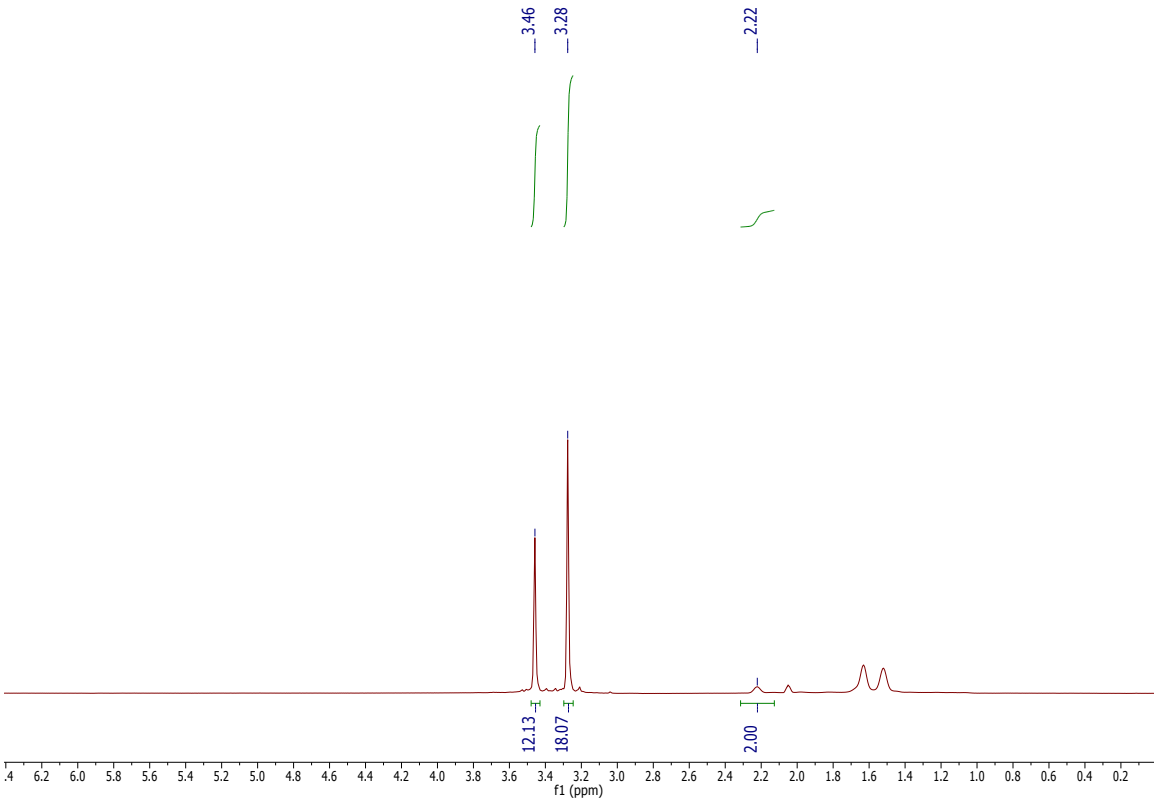

Figure S2. $^{1}H\{^{11}B\}$ NMR of **1[Mg^{2+}]** in acetone-d_6. Integration of antipodal B-H of the carborane (2.22 ppm) and intergration of DME signals (3.46 and 3.28 ppm) is used to determine the number of coordinated DME molecules.

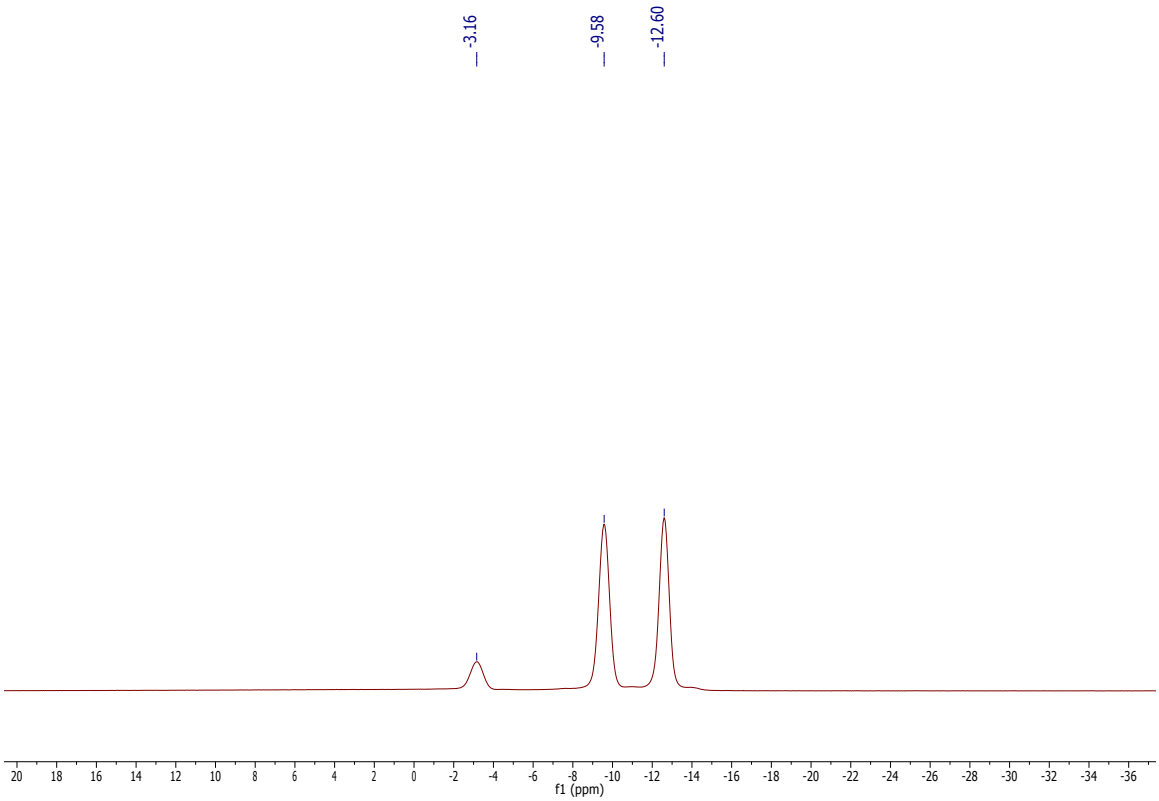

Figure S3. $^{11}B\{^{1}H\}$ NMR of compound **1[Mg^{2+}]** in acetone-d_6.

<u>Synthesis of Ph_2Mg</u>

Ph_2Mg was synthesized according to literature[1] and recrystallized in DME at -30°C (**Note:** Ph_2Mg has 1/2 coordinated DME molecule). ^{1}H NMR (400 MHz, THF-d_8): δ = 7.94 (d, $^{3}J(H,H)$= 6.4 Hz, 2H), δ = 6.87 (dd, $^{3}J(H,H)$= 7.6, 7.2 Hz, 2H), δ = 6.75 (t, $^{3}J(H,H)$= 7. Hz, 1H); $^{13}C\{^{1}H\}$ NMR (300 MHz, DME): δ = 180.4 (ipso *C*H), δ = 143.2 δ = 125.2 δ = 123.1 ppm.

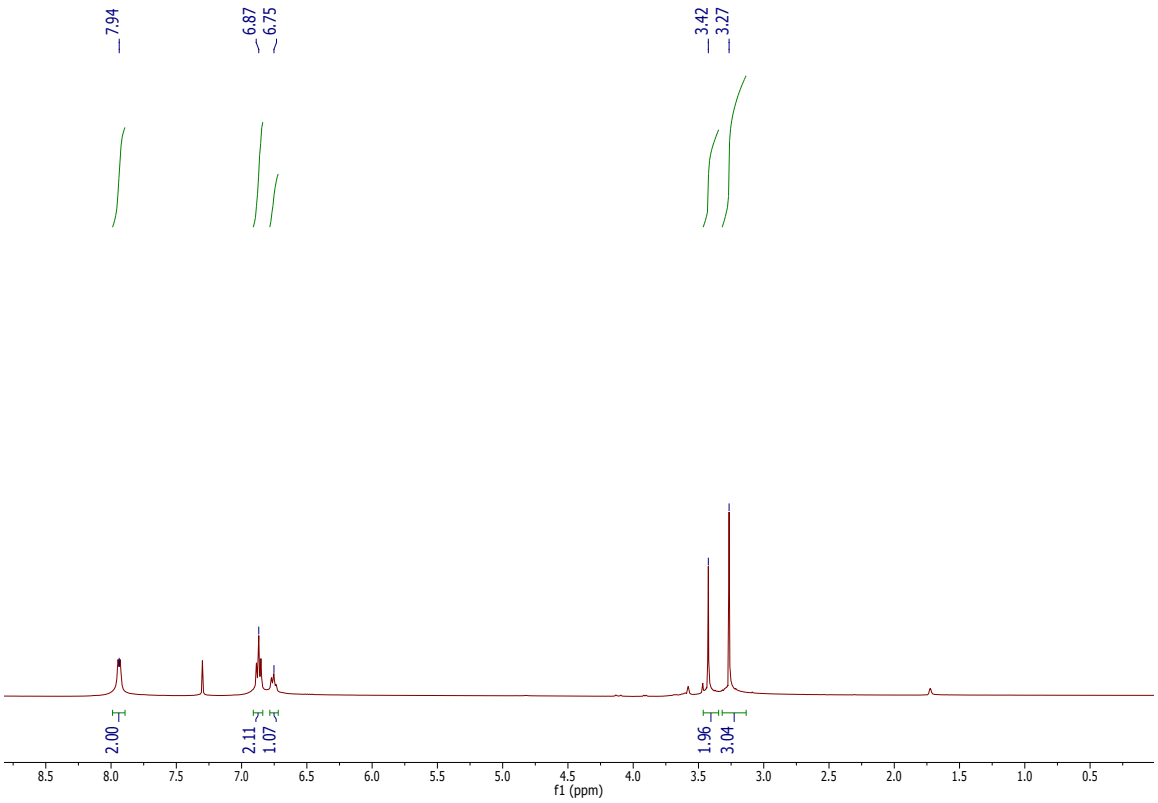

Figure S4. ^{1}H NMR of Ph_2Mg in THF-d_8 (**Note**: Minute amounts of adventitious water in the NMR solvent leads to partial protonolysis of the reactive Mg-Ph bond, which explains the trace of protio benzene in the NMR spectra at 7.30 ppm. Coordinated DME 3.43 ppm, 3.27 ppm).

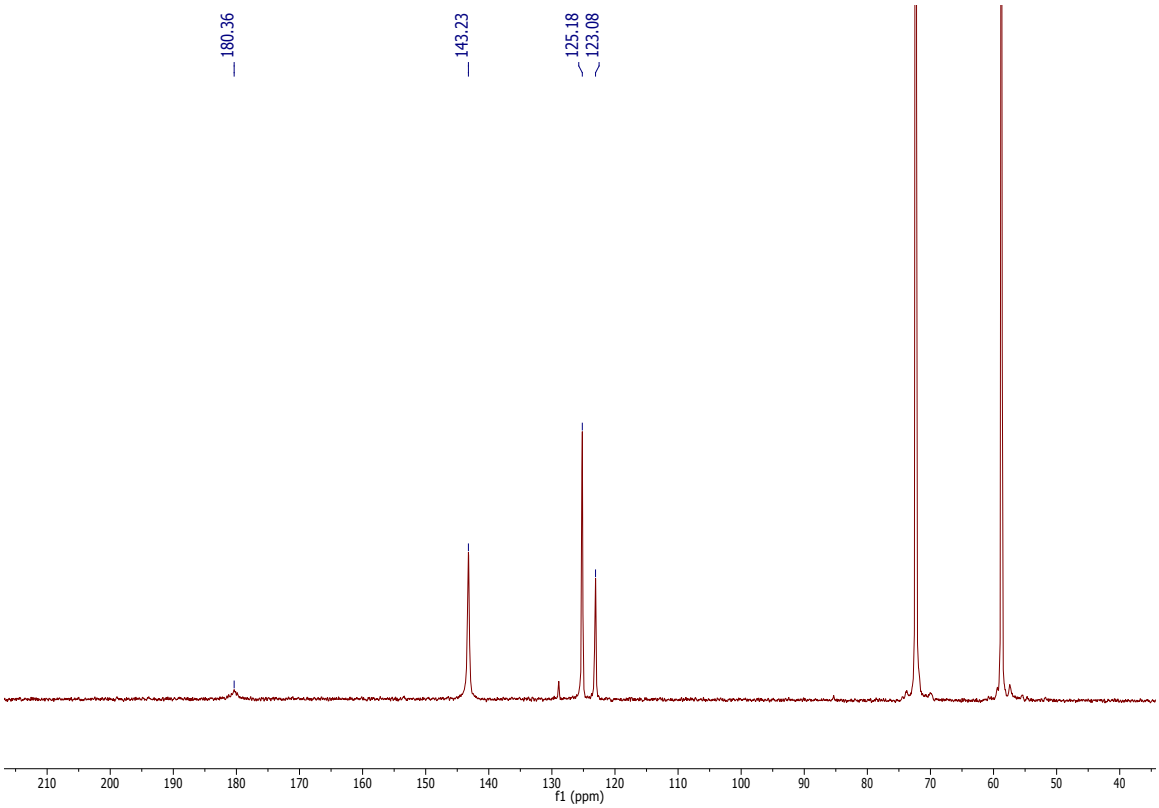

Figure S5. $^{13}C\{^{1}H\}$ NMR of Ph_2Mg in DME (**Note:** Minute amounts of adventitious water in the NMR solvent leads to partial protonolysis of the reactive Mg-Ph bond, which explains the trace of protio benzene in the NMR spectra at 128.9 ppm)

Synthesis of 1[MgPh^{1+}]

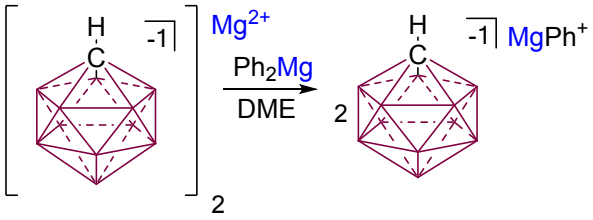

1[Mg^{2+}] **1[MgPh^{1+}]**

Crystalline Ph_2Mg (580 mg, 2.15 mmol) was dissolved in DME and added to a stirring suspension of **1[Mg^{2+}]** (1.25 g, 2.15 mmol) in 10mL DME. Addition of Ph_2Mg instantly solubilizes the suspension. DME is removed under high vacuum, affording **1[MgPh^{1+}]** in 92% yield (1.68g, 3.9 mmol) (**Note:** MgPh cation contains 2 DME molecules coordinated). Crystal suitable for single crystal diffraction was obtained by crystallization in toluene at -35°C. ^{1}H NMR (400 MHz, THF-d_8, 25°C): δ = 7.52 (d, $^{3}J(H,H)$ = 6.40 Hz, 2 H), 6.95 (dd, $^{3}J(H,H)$ = 6.80, 8.61 Hz, 2 H), 6.83 (t, $^{3}J(H,H)$ = 6.80 Hz, 1 H), 2.2-0.85 (bm, 11H, B-*H*) ppm; ^{13}C{^{1}H} NMR (300 MHz, THF-d_8, 25°C): δ = 168.9 (ipso *C*H), 140.0, 124.9, 123.0 ppm; ^{11}B{^{1}H} NMR (96 MHz, DME, 25 °C): δ = -4.2, -10.6, -13.7 ppm.

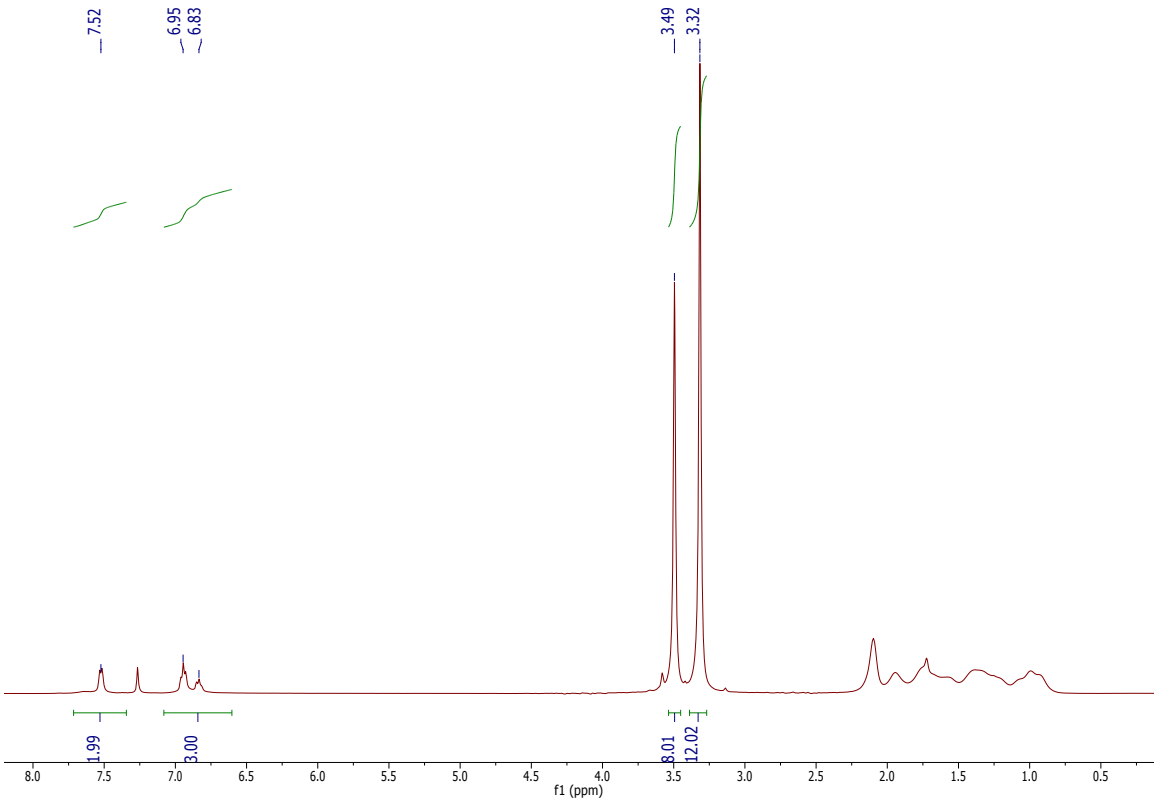

Figure S6. ^{1}H NMR of **1**[MgPh^{1+}] in THF-d_8 (**Note:** Minute amounts of adventitious water in the NMR solvent leads to partial protonolysis of the reactive Mg-Ph bond, which explains the trace of protio benzene in the NMR spectra at 7.26 ppm. Coordinated DME 3.50 ppm, 3.32 ppm).

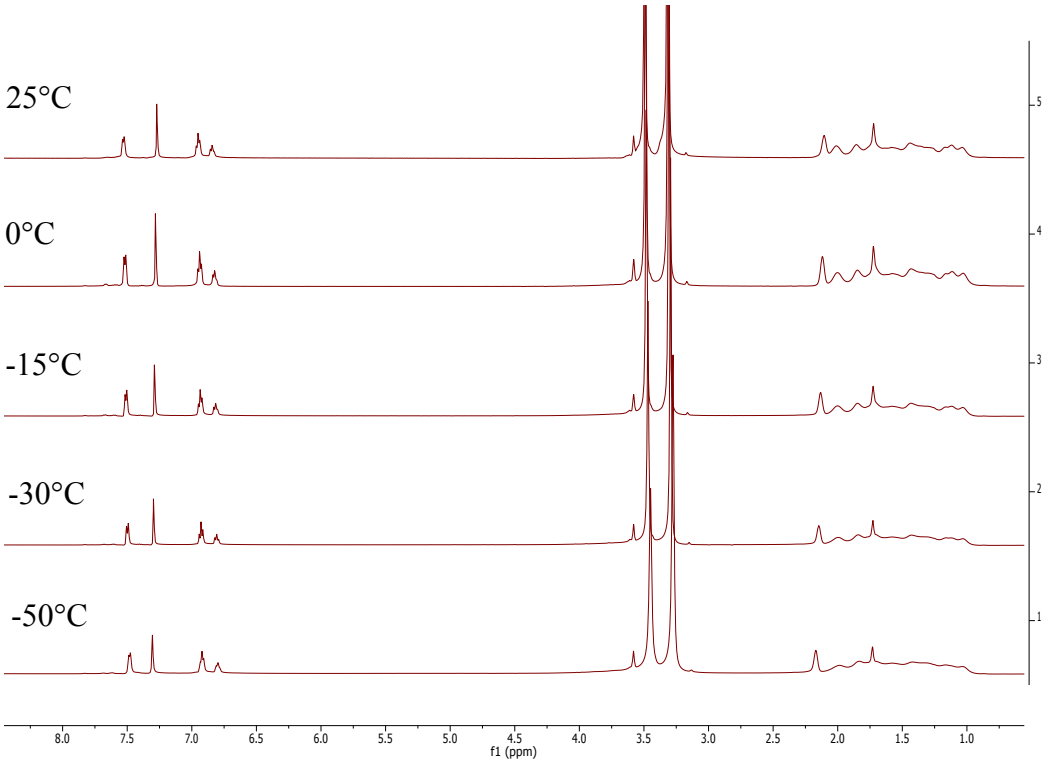

Figure S7. Variable temperature ^{1}H NMR of **1[MgPh^{1+}]** in THF-d_8 (**Note**: Minute amounts of adventitious water in the NMR solvent leads to partial protonolysis of the reactive Mg-Ph bond, which explains the trace of protio benzene in the NMR spectra at 7.26 ppm. Coordinated DME 3.50 ppm, 3.32 ppm).

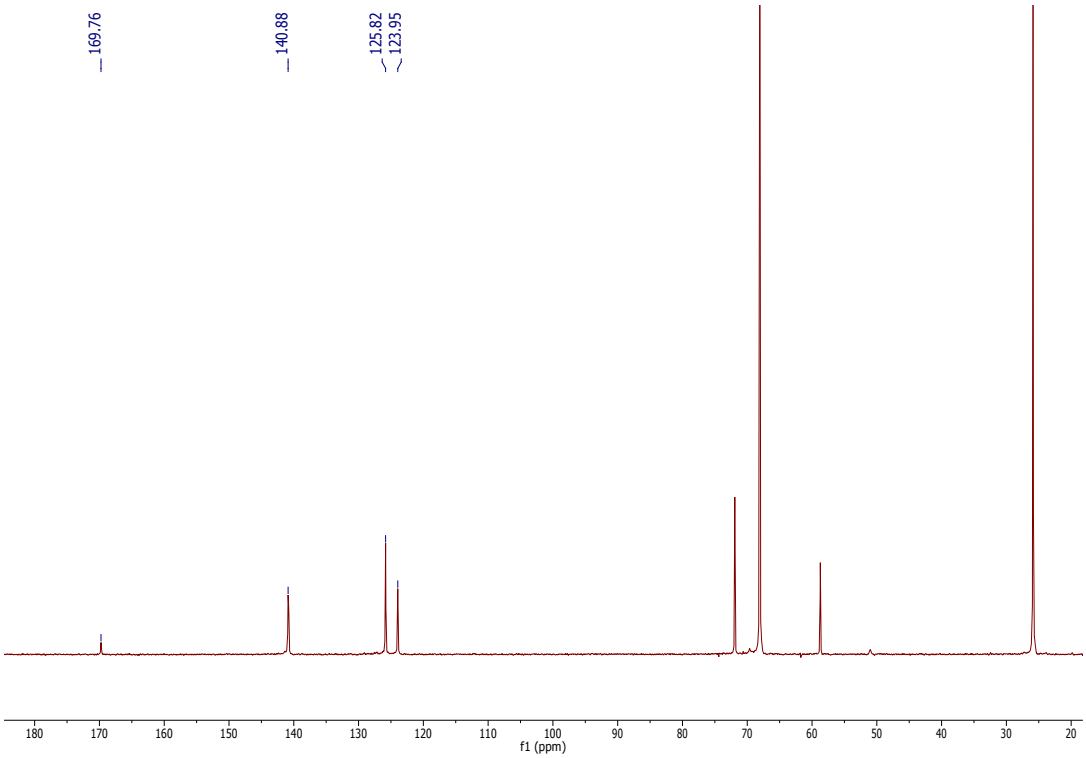

Figure S8. ^{13}C NMR **1**[$MgPh^{1+}$] in THF-d_8 (**Note**: Carbon of carborane is at 51.0 ppm).

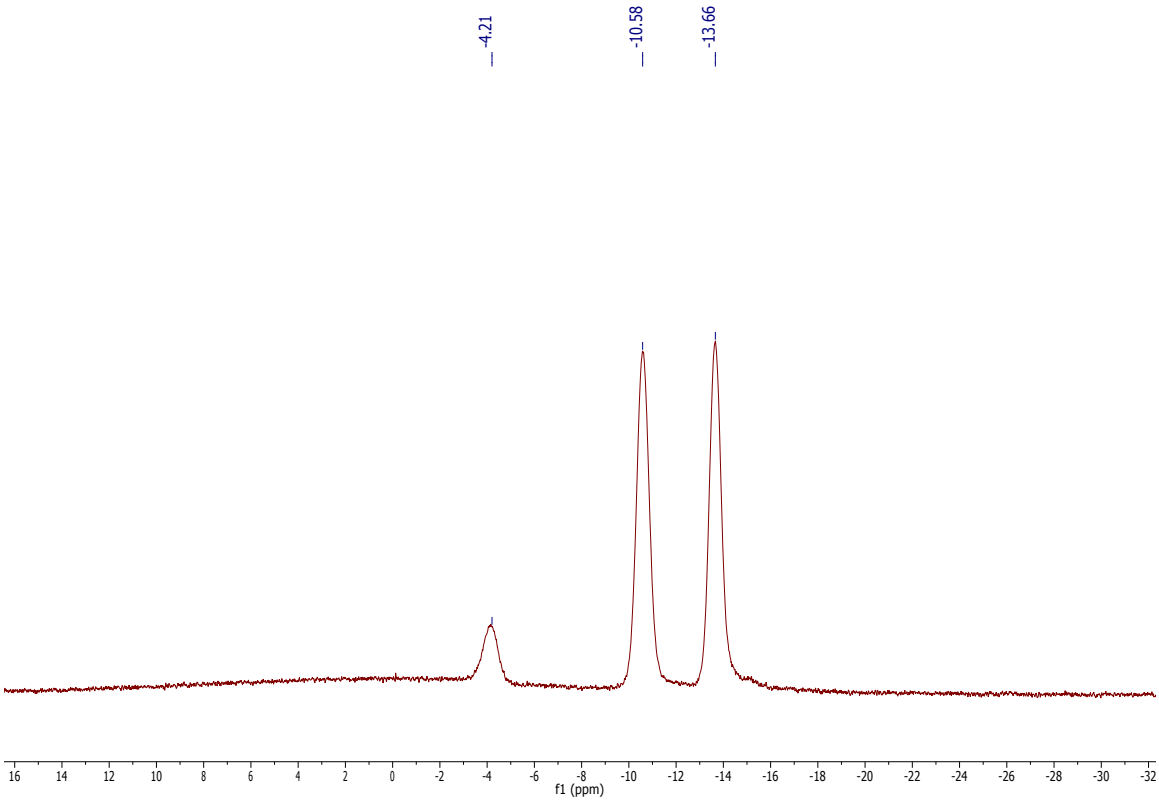

Figure S9. $^{11}B\{^{1}H\}$ NMR of **1**[$MgPh^{1+}$] in DME.

X-Ray Structure Determination

A colorless prism fragment (0.567 x 0.323 x 0.241 mm^3) was used for the single crystal x-ray diffraction study of $[[C_4H_{10}O_2]_2[C_4H_8O][C_6H_5]Mg]^+[CH_{12}B_{11}]^-.[C_7H_8]_2$ (sample vL149SM_0m-5). The crystal was coated with paratone oil and mounted on to a cryo-loop glass fiber. X-ray intensity data were collected at 100(2) K on a Bruker APEX2[2] platform-CCD x-ray diffractometer system (fine focus Mo-radiation, λ = 0.71073 Å, 50KV/30mA power). The CCD detector was placed at a distance of 5.0600 cm from the crystal.

A total of 4800 frames were collected for a sphere of reflections (with scan width of 0.3° in ω, starting ω and 2θ angles of –30°, and ϕ angles of 0°, 90°, 120°, 180°, 240° and 270° for every 600 frames, and 1200 frames with ϕ-scan from 0-360°, 60 sec/frame exposure time). The Bruker Cell_Now program[3] was used to obtain the two different orientation matrices of the rotational twin components (Twin law is 180° rotation about the 1 0 1 real axis). These matrices were imported into the APEX2 program for Bravais lattice determination and initial unit cell refinement. The frames were integrated using the Bruker SAINT software package[4] and using a narrow-frame integration algorithm. Based on a monoclinic crystal system, the integrated frames yielded a total of 4946 unique independent reflections [maximum 2θ = 43.932° (0.95 Å resolution), data completeness = 100%] and 4557 (92.1%) reflections were greater than 2σ(I). The unit cell parameters were, **a** = 16.659(3) Å, **b** = 13.261(3) Å, **c** = 18.213(4) Å, β = 97.572(3)°, V = 3988.1(14) $Å^3$, Z = 4, calculated density D_c = 1.134 g/cm^3. Absorption corrections were applied (absorption coefficient μ = 0.082 mm^{-1}; min/max transmission = 0.955/0.981) to the raw intensity data using the Bruker TWINABS program[5].

The Bruker SHELXTL software package[6] was used for phase determination and structure refinement. Using the first twin domain HKL 4 intensity data, the distribution of intensities and systematic absent reflections indicated one possible space group, P2(1)/n. The space group P2(1)/n (#14) was later determined to be correct. Direct methods of phase determination followed by two Fourier cycles of refinement led to an electron density map from which most of the non-hydrogen atoms were identified in the asymmetry unit of the unit cell. With subsequent isotropic refinement, all of the non-hydrogen atoms were identified. The combined (major and minor components) HKLF 5 intensity dataset was used in the final structure refinement. There was one cation of $[[C_4H_{10}O_2]_2[C_4H_8O][C_6H_5]Mg]^+$, one anion of $[CH_{12}B_{11}]^-$, and two toluene molecules present in the asymmetry unit of the unit cell. The rotational twin law was 180^o rotation about the 1 0 1 real axis. The major/minor twin component ratio was 51%/49%. The alert levels A and B are due to the poor crystal quality with low resolution data. Attempts to model the possible toluene, cation and anion disorder failed because of poor quality data with low resolution.

Atomic coordinates, isotropic and anisotropic displacement parameters of all the non-hydrogen atoms were refined by means of a full matrix least-squares procedure on F^2. The H-atoms were included in the refinement in calculated positions riding on the atoms to which they were attached. The refinement converged at R1 = 0.0985, wR2 = 0.2405, with intensity, $I>2\sigma(I)$. The largest peak/hole in the final difference map was 0.438/-0.381 e/$Å^3$.

Table 1. Crystal data and structure refinement for vL149SM_0m-5.

Identification code	vL149SM_0m-5	
Empirical formula	C33 H61 B11 Mg O5	
Formula weight	681.03	
Temperature	100(2) K	
Wavelength	0.71073 Å	
Crystal system	Monoclinic	
Space group	P 21/n (#14)	
Unit cell dimensions	a = 16.659(3) Å	α = 90°.
	b = 13.261(3) Å	β = 97.572(3)°.
	c = 18.213(4) Å	γ = 90°.
Volume	3988.1(14) $Å^3$	
Z	4	
Density (calculated)	1.134 Mg/m^3	
Absorption coefficient	0.082 mm^{-1}	
F(000)	1464	
Crystal size	0.567 x 0.323 x 0.241 mm^3	
Theta range for data collection	1.778 to 21.966°.	
Index ranges	-17<=h<=17, 0<=k<=13, 0<=l<=19	
Reflections collected	15800	
Independent reflections	4946 [R(int) = 0.0613]	
Completeness to theta = 25.242°	100.0 %	
Absorption correction	Semi-empirical from equivalents	
Refinement method	Full-matrix least-squares on F^2	
Data / restraints / parameters	4946 / 30 / 458	
Goodness-of-fit on F^2	1.159	
Final R indices [I>2sigma(I)]	R1 = 0.0985, wR2 = 0.2405	
R indices (all data)	R1 = 0.1065, wR2 = 0.2464	
Extinction coefficient	n/a	
Largest diff. peak and hole	0.438 and -0.381 $e.Å^{-3}$	

Synthesis of Mo_6S_8

All reagents were purchased from commercial vendors without further purification. In a typical synthesis of Mo_6S_8, stoichiometric amounts of anhydrous copper(II) chloride ($CuCl_2$, 0.3442 g, 2.56 mmol, Sigma Aldrich 99.995%) and ammonium tetrathiomolybdate ($(NH_4)_2MoS_4$, 2.000 g, 7.68 mmol; Fisher Scientific 99.99%) were dissolved in 65 mL N,N-Dimethylformamide (DMF, Sigma Aldrich 99.8%) and the mixture was stirred for 30 min at room temperature. The resultant solution was then heated at 90 °C for 6 hours under continuous argon bubbling. After the reaction was completed, the solution was filtered, and then 325 mL THF (1:5 by volume) was added immediately to the filtrate to initiate precipitation. The precipitate was collected by centrifuge, washed with THF and dried in the vacuum oven at 150 °C overnight. The dried solid agglomerate was then ground and heated in a tube furnace at 1000 °C for 7 hour under reducing environment (95 vol.% argon and 5 vol.% H_2) to yield Chevrel phase $Cu_2Mo_6S_8$. The obtained $Cu_2Mo_6S_8$ was then added into 20 mL 6M HCl solution. Oxygen was bubbled into the solution for 8 hours while stirring to leach out Cu to yield Mo_6S_8. After the reaction, the obtained Mo_6S_8 was centrifuged, washed with adequate amount of deionized water, and dried in vacuum oven at 50 °C overnight.

Electrochemical Analysis

The cyclic voltammetry (CV) of Mg deposition-dissolution and the galvanostatic Mg deposition were performed in three-electrode cells with a Gamry potentiostat/galvanostat/ZRA (Interface 3000) using Pt (GC, Ti, SS, Ni) working electrode and two Mg strips (Alfa Aesar 99.9%) as the counter and the reference electrodes, respectively. A constant current density of 0.5 mA cm^{-2} was applied on Pt substrate for 8 hours in electrochemical Mg deposition experiment.

The conductivity of the 1[$MgPh^{1+}$] electrolyte was obtained from the resistance measurement in a cell with two parallel Pt electrodes. The cell constant was obtained through calibration using standard aqueous KCl solutions. The resistance was measured with a Gamry potentiostat/galvanostat/ZRA (Interface 1000).

For coin cells assembly, Mg foil with 0.25 mm thickness (Alfa Aesar 99.9%) was used as the anode. Cathode was fabricated by coating Mo_6S_8 slurry onto carbon paper current collector. The slurry was made by mixing 80 wt.% Mo_6S_8, 10 wt.% carbon black, and 10 wt.% polyvinylidene fluoride in N-Methyl-2-pyrrolidone via a mechanical mixer for 5 min in an argon-filled glovebox. CR2032 coin cells were assembled in the argon-filled glovebox. The galvanostatic charge-discharge experiments of the coin cell batteries were performed on an Arbin battery test station, and the CV analysis of the Mg-Mo_6S_8 coin cells was conducted on a Gamry Interface 1000 with a scan rate of 0.1 mV s^{-1}.

Galvanostatic cycling method[7] was used for the average Mg deposition/stripping coulombic efficiency measurement on Ti, Ni, and SS working electrodes. Excess of Mg was first galvanostatically deposited on the metal electrodes with a 1 C cm^{-2} capacity (1 mA cm^{-2} for 1000 seconds), which was followed by galvanostatic cycling with a 0.25 C

cm^{-2} capacity (1 mA cm^{-2} for 250 seconds). The average coulombic efficiency (ACE) was determined by the number of cycles required to completely consume the excess Mg, using the following formula: $ACE=100\times NQ_{cy}/(NQ_{cy}+Q_{ex})$ (N is the number of cycles, Q_{cy}=0.25 C cm^{-2}, and Q_{ex}=1 C cm^{-2}). This determination of ACE of Mg deposition/stripping is more realistic to reflect the practical Mg battery design with excess of Mg at the anode.

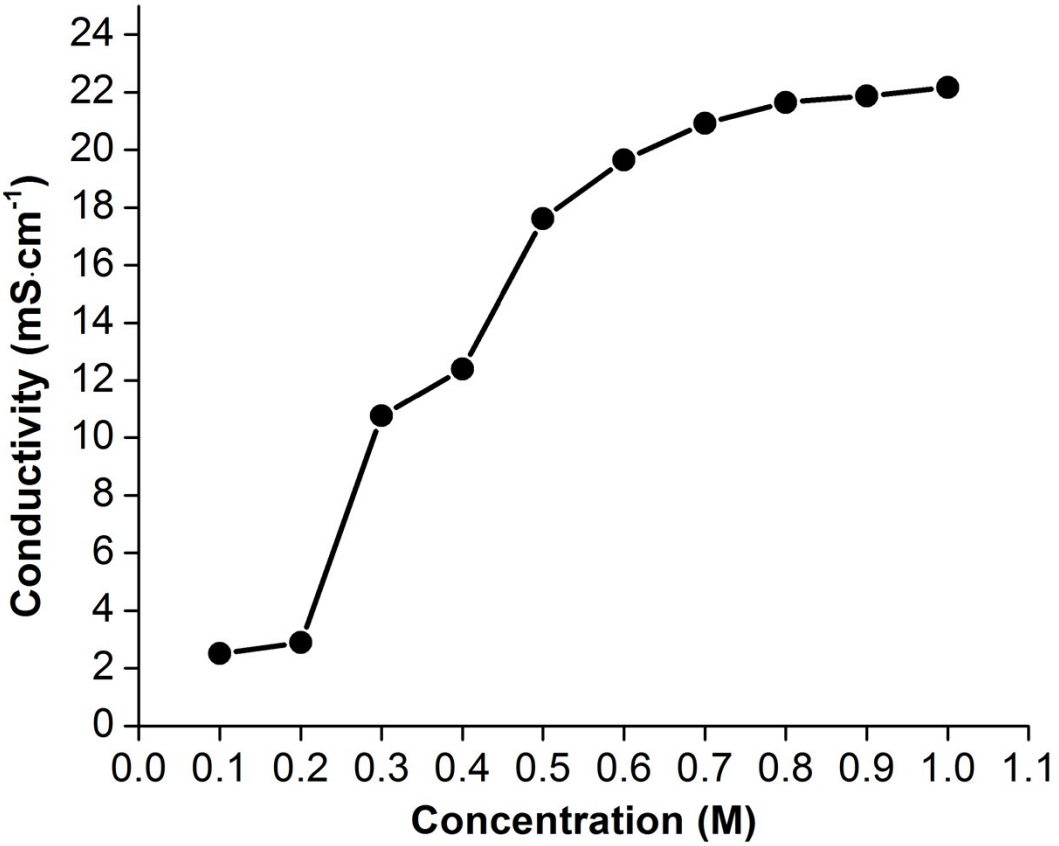

Figure S10. Room temperature conductivity of **1**[$MgPh^{1+}$] in DME as function of salt concentration.

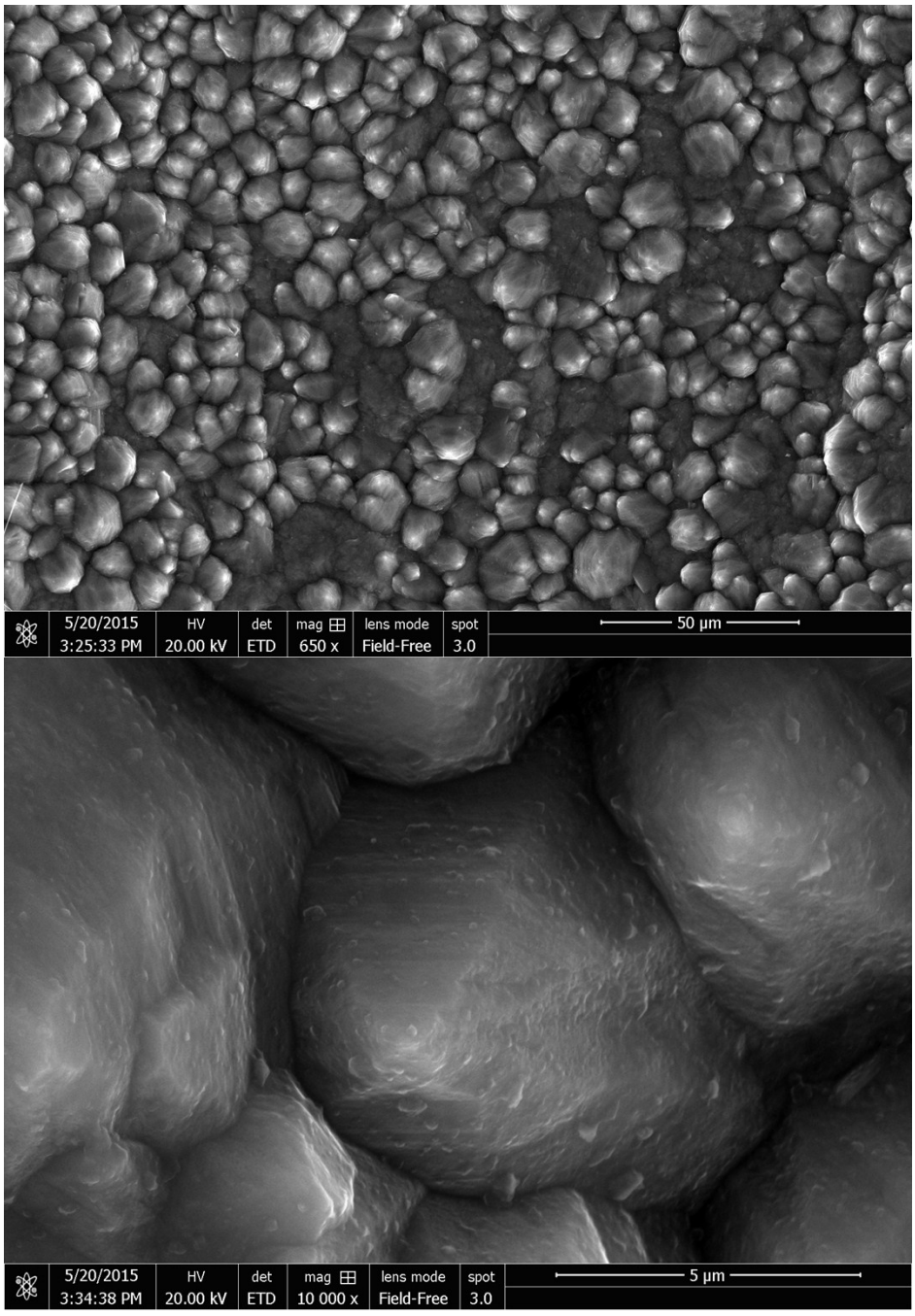

Figure S11. Scanning electron microscopy (SEM) images of Mg deposited on Pt working electrode galvanostatically with a 0.5 mA cm^{-2} current density. SEM was performed with a Nova NanoSEM 450.

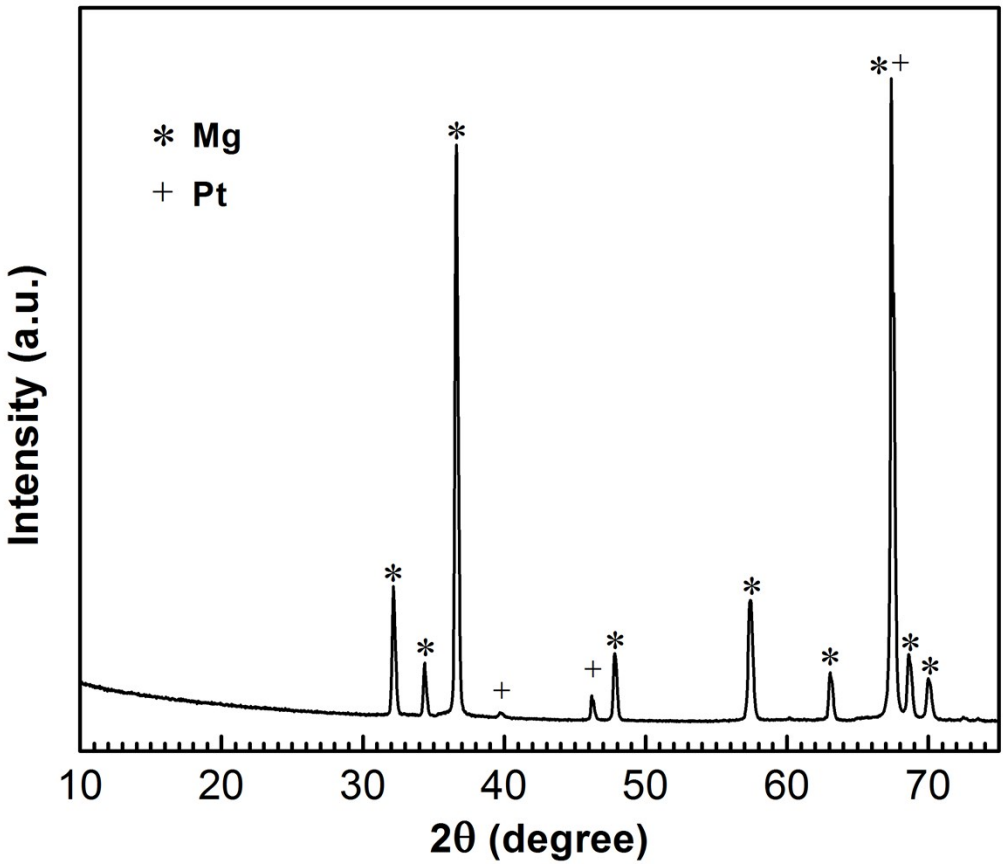

Figure S12. The X-ray diffraction (XRD) pattern of Mg deposited on Pt working electrode. The XRD was conducted using PANalytical EMPYREAN instrument (45 kV/40 mA) with a Cu-Kα source.

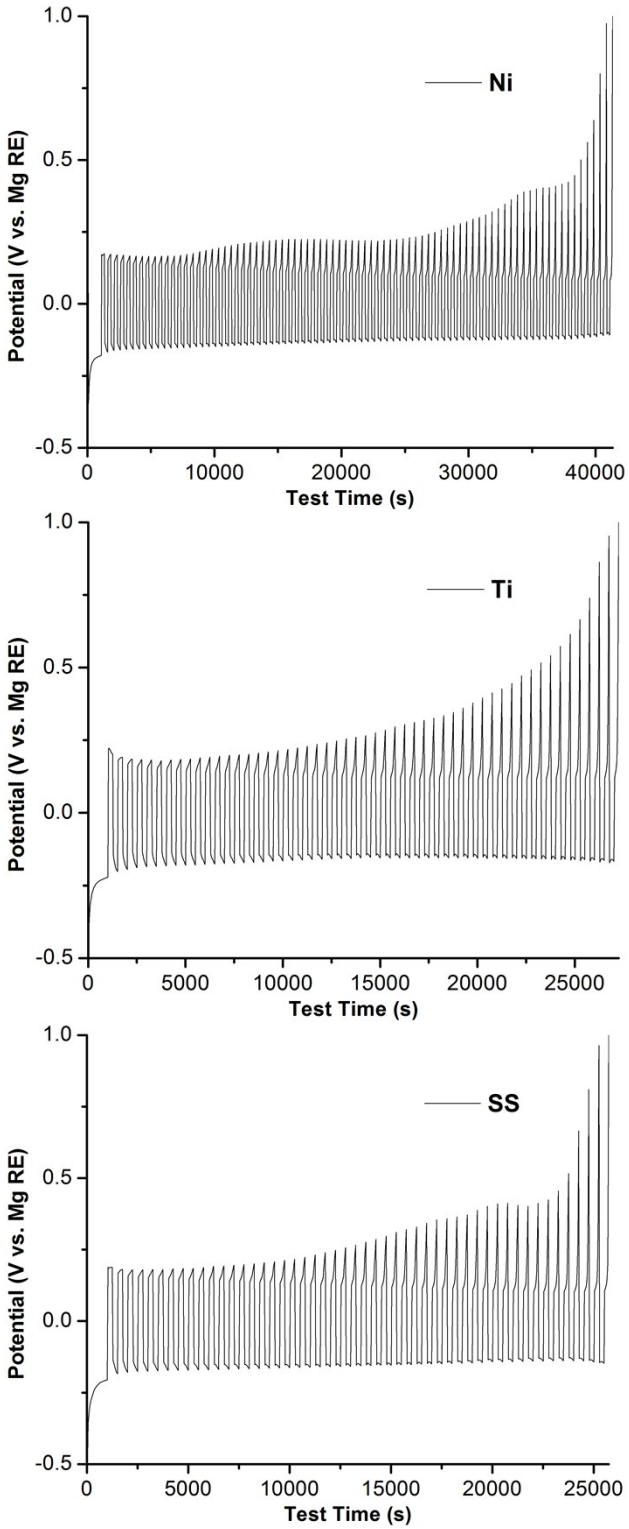

Figure S13. Galvanostatic cycling for average coulombic efficiency measurement on Ni, Ti, and SS. The ACE for Ni, Ti, and SS are 95.3%, 93.7% and 91.7%, respectively.

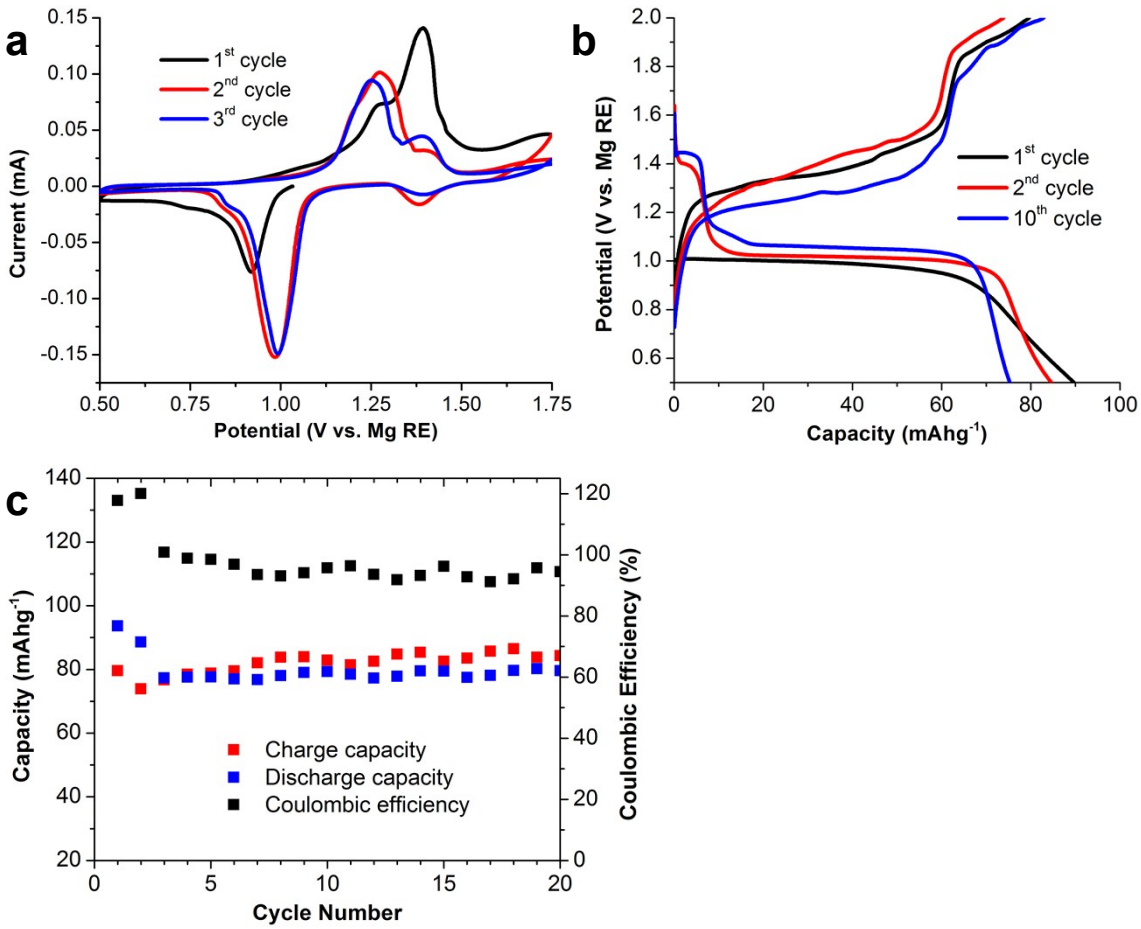

Figure S14. (a) CV (0.1 mV s^{-1} scan rate), (b) selected galvanostatic charge-discharge curves (0.1C), and (c) cycle stability (0.1C) of Mg battery with Mo_6S_8 cathode.

Reference:

[1]. C. G. Screttas, M. Micha-Screttas, *Journal of Organometallic Chemistry* **1985**, *292*, 325-333.

[2]. ***APEX 2,*** version 2014.1.1, Bruker (2014), Bruker AXS Inc., Madison, Wisconsin, USA.

[3]. ***CELL_NOW***, version 2008/4, Bruker (2012), Bruker AXS Inc., Madison, Wisconsin, USA.

[4]. ***SAINT,*** version V8.34A, Bruker (2012), Bruker AXS Inc., Madison, Wisconsin, USA.

[5]. ***TWINABS***, version 2012/1, Bruker (2012), Bruker AXS Inc., Madison, Wisconsin, USA.

[6]. ***SHELXTL,*** version 2013/4, Bruker (2013), Bruker AXS Inc., Madison, Wisconsin, USA.

[7]. P. C. Howlett, D. R. MacFarlane, and A. F. Hollennkamp, *Electrochemical and Solid-State Letters* **2004**, *7*, A97-A101.